Korean J. Chem. Eng., 33(1), 170-177 (2016)
DOI: 10.1007/s11814-015-0111-1

pISSN: 0256-1115
eISSN: 1975-7220

Removal of UO_2^{2+} from aqueous solution using halloysite nanotube-Fe_3O_4 composite

Wenfang He, Yuantao Chen†, Wei Zhang, Chunlian Hu, Jian Wang, and Pingping Wang

Department of Chemistry, Qinghai Normal University, Xining 810008, P. R. China
(*Received 13 October 2014 • accepted 26 May 2015*)

Abstract−Halloysite nanotubes (HNTs) were modified with Fe_3O_4 to form novel magnetic HNTs-Fe_3O_4 composites, and the composites were characterized by X-ray diffraction (XRD), transmission electron microscope (TEM), Fourier transform infrared spectroscopy (FT-IR) and vibrating sample magnetometer (VSM). The as-obtained results indicated that Fe_3O_4 nanoparticles were successfully installed on the surface of HNTs. The adsorption of UO_2^{2+} on HNTs-Fe_3O_4 was investigated as a function of solid content, contact time, pH, ionic strength and temperature by batch experiments. The consequences revealed that the adsorption of UO_2^{2+} onto HNTs-Fe_3O_4 was strongly dependent on pH and ionic strength. Equilibrium data fitted well with the Langmuir isotherm. The experimental results demonstrated that the adsorbents with HNTs-Fe_3O_4 had the largest adsorption capacity of 88.32 mg/g for UO_2^{2+}.

Keywords: Halloysite Nanotubes-Fe_3O_4, Adsorption, UO_2^{2+}, Modification, pH

INTRODUCTION

Water radioactive pollution is a serious environmental problem. Uranium (UO_2^{2+}), a representative actinide element, is released into the environment as an important radionuclide in radioactive wastewater [1]. Due to the long half-life ($t_{1/2}(^{235}U)=7.04\times10^8$ a; $t_{1/2}(^{238}U)$ 4.47×10^9 a), the release of UO_2^{2+} into the environment can cause great harm to human health, the ecosystem, and agriculture. Therefore, the removal of UO_2^{2+} from aqueous solution is necessary and urgent.

At present, some measures are being used to the remove UO_2^{2+} from aqueous solution. Those methods such as solvent extraction, chemical precipitation, ion-exchange, membrane separation, adsorption, anti-dialysis and electrodialysis have made achievements in the field of pollution control. Among them, adsorption has proven to be one of the most promising techniques for the removal of UO_2^{2+} from aqueous solution owing to its high efficiency, low energy requirement, environmentally friendly process and economic feasibility. The removal of UO_2^{2+} from aqueous solution by using different kinds of adsorbents has been studied extensively [2-4], and the results indicate that the adsorption of UO_2^{2+} is mainly dominated by ion exchange and outer-sphere surface complexation at low pH values, whereas by inner-sphere surface complexation or precipitation at high pH values [5]. So far, many adsorbents have been used to removal of UO_2^{2+} including carbon nanotubes [6-8], hematite [9], Na-rectorite [10-12], diatomite [13] and graphene [14,15]. However, these adsorbents have high cost and low efficiency. Prior studies [16] showed that clays were promising adsorbents due to low cost, abundant resources, simply operation, high specific surface area and high adsorption capacity.

Halloysite ($Al_2(OH)_4Si_2O_5\cdot2H_2O$) is a kind of two-layered aluminosilicate clay with a predominantly hollow tubular structure in the submicron range, which can be obtained from the natural environment [17]. The layers curl into tubules, which most likely is due to the mismatch in the areas of one alumina octahedron sheet and one silica tetrahedron sheet making up the 1 : 1 layer [18]. Studies [25] have shown that the external surface of halloysite consists of tetrahedral Si-O-Si groups and internal surface composed of octahedral Al-OH groups. It has negative charges on its surface at wide pH range, which leads it to have high capacity to absorb UO_2^{2+} from aqueous solutions. In previous studies, HNTs have been widely used in catalysis, electronics, biomedicine and functional materials [26]. Currently, HNTs have been proven to have the ability to remove heavy metal ions. The adsorption of UO_2^{2+} has been studied in our group. Xiao [19] and Chi [5] have used bentonite and attapulgite as adsorbents to remove UO_2^{2+} from aqueous solution. However, we found that the adsorbent could disperse in the water and separate inconvenience from aqueous solution, which was owing to hydroxyl groups on the surface. The combination of magnetic separation technology and adsorption process has received widespread attention due to the separable ability from aqueous solution by the application of external magnetic field [20,21]. However, no investigations on the adsorption of UO_2^{2+} on HNTs-Fe_3O_4 have been reported. Therefore, a new kind of magnetic adsorbent HNTs-Fe_3O_4 is a promising adsorbent that opens new possibilities for the achievement of desirable absorptivity [22].

Based on the above background, our aim was to prepare and characterize halloysite nanotubes-Fe_3O_4 composites and to investigate how they can be utilized for the removal of UO_2^{2+} from aqueous solution.

EXPERIMENTAL AND METHODS

1. Materials

The halloysite nanotube (HNTs) sample was obtained from Guangdong Province, China. UO_2^{2+} stock solution was prepared by dissolving uranyl nitrate hexahydrate ($UO_2(NO_3)_2\cdot6H_2O$) in Milli-Q water. All other reagents in the experiments were purchased as ana-

†To whom correspondence should be addressed.
E-mail: chenyt@qhnu.edu.cn

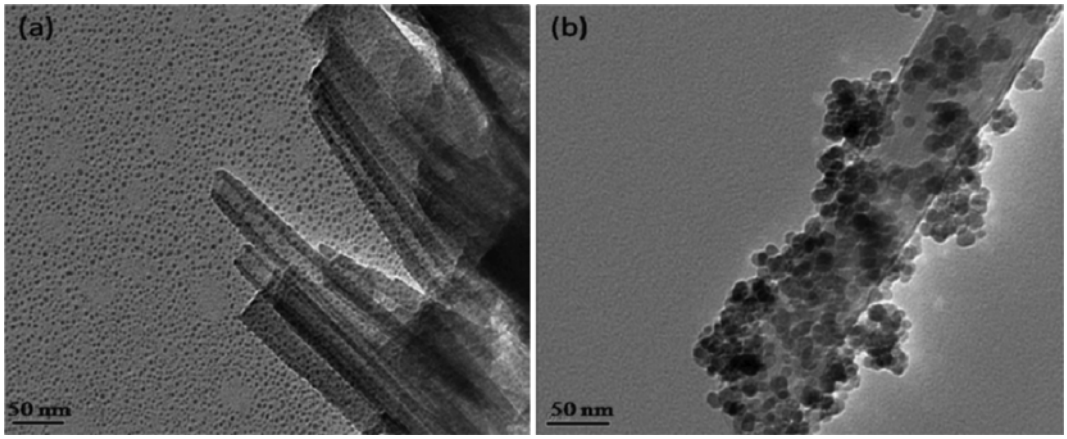

Fig. 1. TEM micrographs of HNTs (a) and HNTs–Fe_3O_4 (b).

lytical purity and used without any further purification.

2. Preparation of HNTs-Fe_3O_4

The magnetic composites were prepared from a suspension of 1.5 g halloysite in a 150 mL solution of 2.9 g $FeCl_3 \cdot 6H_2O$ and 1.5 g $FeSO_4 \cdot 7H_2O$ at 70 °C under N_2 conditions. NaOH solution (30 mL, 0.025 mol/L) was added dropwise to prepare iron oxides. After the addition of NaOH solution, the pH of the final mixtures was controlled in the range of 10-11 and stirred for 1 h. To promote the complete growth of the composite crystals, the reaction was at 70 °C for 4 h under constant magnetic stirring. Finally, the mixture was washed six times with distilled water. Then the composites were dried under vacuum at 70 °C for 6 h. The resulting magnetic halloysite nanocomposite is referred to as HNTs-Fe_3O_4.

3. Characterization of the Adsorbents

The surface functional groups in the HNTs and HNTs-Fe_3O_4 were characterized by FT-IR, XRD. TEM was used to identify the morphology and microscopic structure of HNTs and HNTs-Fe_3O_4. The magnetic properties of HNTs-Fe_3O_4 were measured on a VSM.

4. Adsorption Experiments Procedures

Effects of the concentration of the UO_2^{2+}, the pH of the medium, the temperature and the contact time on the adsorption were studied. Adsorption experiments were conducted using the polyethylene centrifuge tubes under ambient conditions containing 6 g/L of HNTs-Fe_3O_4 and the $UO_2(NO_3)_2 \cdot 6H_2O$ (1 mmol/L). The polyethylene centrifuge tubes were placed on a thermostated shaker with a shaking of 180 rpm for 24 h and then centrifuged at 8,000 rpm for 30 min to separate the solid from liquid phases. The concentration of UO_2^{2+} was detected with UV-VIS spectrophotometer at λ_{max} of 671 nm. The amount of UO_2^{2+} adsorbed on Fe_3O_4-HNTs was calculated from the difference between the initial concentration and the equilibrium one. The adsorption efficiency and the distribution coefficient K_d was calculated by using the following equations, respectively:

$$\text{Sorption}\% = \frac{C_0 - C_{eq}}{C_0} \times 100\% \quad (1)$$

$$K_d = \frac{C_0 - C_{eq}}{C_0} \times \frac{V}{m} \quad (2)$$

where C_0 is the initial concentration, C_{eq} is the final one in supernatant after centrifugation, m is the mass of HNTs-Fe_3O_4 and V is the volume of the suspension.

RESULTS AND DISCUSSION

1. Characterizations

1-1. TEM

The TEM images of original HNTs and HNTs-Fe_3O_4 are shown in Fig. 1. Fig. 1(a) shows the halloysite nanotubes with a smooth surface. Fig. 1(b) shows that the Fe_3O_4 nanoparticles are attached on the inside wall of halloysite nanotubes. The attachment can be related to the structures of HNTs, such as the large surface area, large pore volume and adequate hydroxyl groups, which make UO_2^{2+} to access and adsorb on the surface easily [23]. It illustrates that magnetic Fe_3O_4 nanoparticles are successfully installed on the surface of HNTs.

1-2. FT-IR

The FT-IR spectrum of HNTs-Fe_3O_4 is shown in Fig. 2. According to the FT-IR spectrum, the double peaks at 3,699 and 3,622

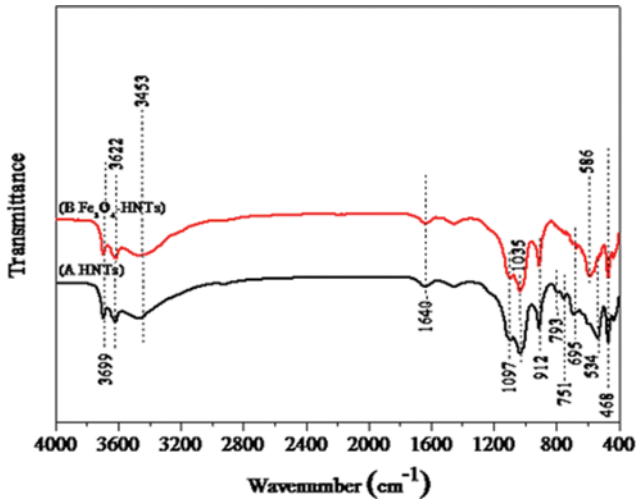

Fig. 2. FTIR spectra of HNTs and HNTs-Fe_3O_4.

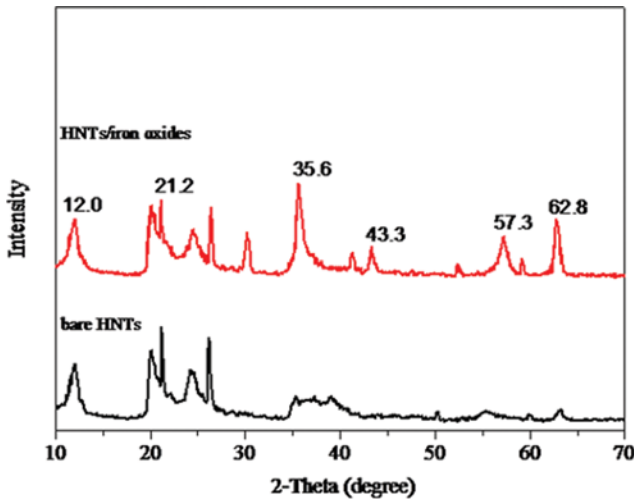

Fig. 3. XRD patterns of original HNTs and HNTs-Fe_3O_4.

cm^{-1} are due to the stretching vibrations of hydroxyl groups at the surface of HNTs [24]. The peaks at 468, 534 and 912 cm^{-1} are attributed to the deformation of Si-O-Si, deformation of Al-O-Si and O-H deformation of inner hydroxyl groups, respectively [25]. The peaks at 1,097 and 1,035 cm^{-1} correspond to the stretching vibrations of Si-O groups in HNTs. The peak at 586 cm^{-1} is due to the stretching vibrations of Fe-O-Fe groups [23].

1-3. XRD

The XRD patterns of the HNTs and HNTs-Fe_3O_4 are shown in Fig. 3. For bare HNTs, the diffraction peaks are at 2θ values of 12.0, 20.1, 21.2, 24.1, 26.2, 35.3, 39.1, 55.2, and 63.3. The broad diffraction peaks manifest that the bare HNTs are in small crystal size and poor crystallinity degree [26]. Compared with bare HNTs, the XRD pattern of HNTs-Fe_3O_4 displays five new peaks at 2θ values of about 30.2, 35.6, 43.3, 57.3, and 62.8, as marked in Fig. 3. These peak positions and relative peak intensities correspond to the characteristic peaks of Fe_3O_4 [27]. Therefore, it indicates that magnetic Fe_3O_4 nanoparticles were successfully installed on the surface of HNTs.

1-4. VSM

Fig. 4(A) shows the magnetization of HNTs-Fe_3O_4 as a function of the applied magnetic field. Magnetization increased with an increase in the magnetic field. HNTs-Fe_3O_4 has good magnetic properties with the saturation magnetization (28.67 emu/g) and shows an extremely small hysteresis loop and low coercivity, as is typically characteristic of superparamagnetic particles [28,29]. Fig. 4(B) shows the separation behavior of HNTs-Fe_3O_4. When a permanent magnetic field was applied, the magnetic HNTs-Fe_3O_4 particles were attracted to the wall of vial and the dispersion became clear and transparent.

2. Effect of Solid Content

Adsorption efficiency and distribution coefficient K_d of UO_2^{2+} on HNTs-Fe_3O_4 as a function of solid content is shown in Fig. 5. The adsorption efficiency increases from 6.5% to 87.78% when the dosage of adsorbent increases from 0.29 to 1.16 mg. The removal of UO_2^{2+} from aqueous solution increases obviously with increasing solid content. As can be seen, the distribution coefficient increases slightly with the increasing concentration of HNTs-Fe_3O_4. Generally, the K_d value is independent of solid content, but we can

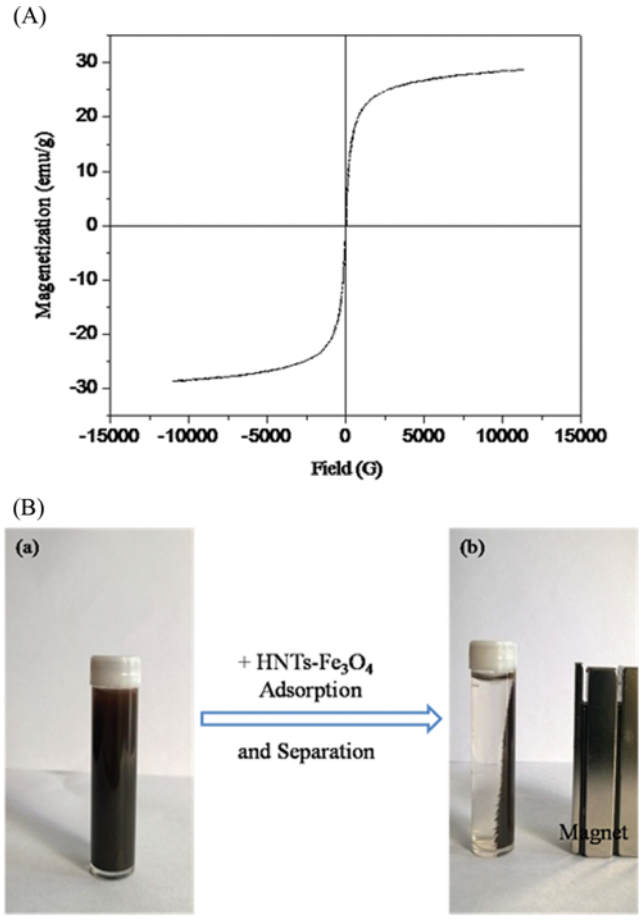

Fig. 4. (A) Magnetic hysteresis cycles for HNTs-Fe_3O_4, (B) separation of Fe_3O_4-HNTs from solution by a magnet, (a) UO_2^{2+}+ HNTs-Fe_3O_4 solution, (b) Magnetic separation after adsorption onto HNTs-Fe_3O_4.

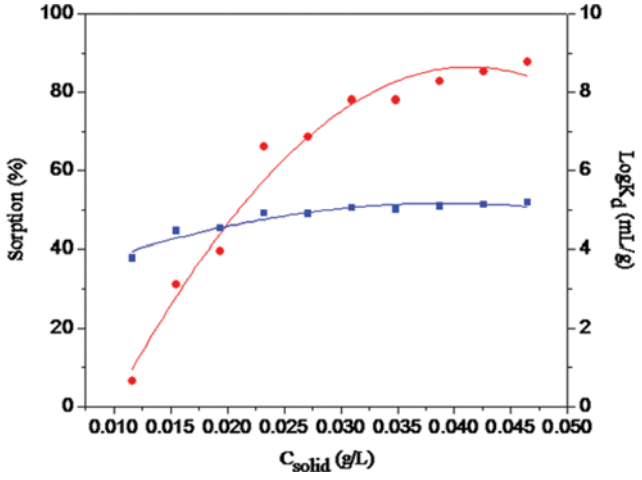

Fig. 5. Adsorption of UO_2^{2+} on HNTs-Fe_3O_4 as a function of solid content (T=293.15 K, pH=5.5±0.1, C_0 (UO_2^{2+})=6.452×10^{-6} mol/L, I=0.01 M NaCl).

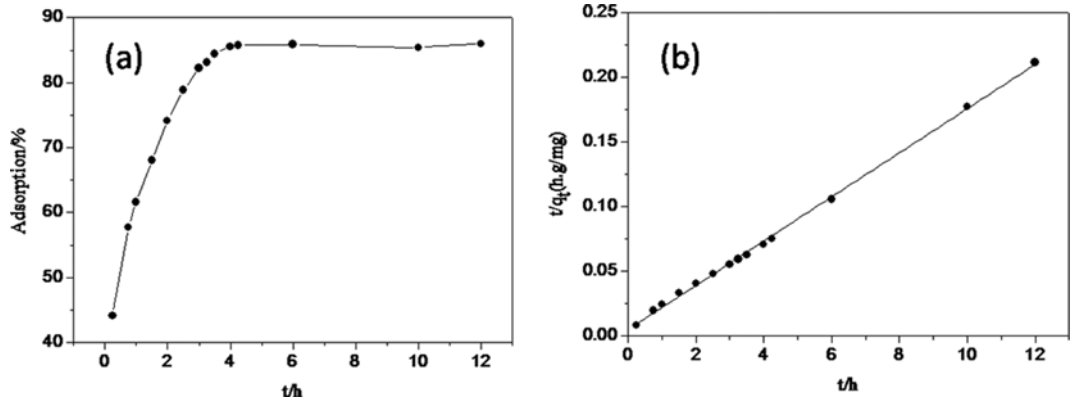

Fig. 6. Effect of contact time on the adsorption of UO_2^{2+} on HNTs-Fe_3O_4. (a) Plot of q_t vs. t for UO_2^{2+} adsorption. (b) Plot of t/q_t vs. t for the pseudo-order model (T=293.15 K, pH=5.5±0.1, C_0 (UO_2^{2+})=6.452×10^{-6} mol/L, I=0.01 M NaCl).

see that the K_d value is dependent on the HNTs-Fe_3O_4 content. With the increasing of HNTs-Fe_3O_4 content, the removal rate of UO_2^{2+} increases and thereby the concentration of free UO_2^{2+} remaining in solution decreases markedly. Therefore, the UO_2^{2+} K_d value increases slightly with increasing of HNTs-Fe_3O_4 content [30].

3. Effect of Contact Time

The adsorption of UO_2^{2+} on HNTs-Fe_3O_4 as a function of contact time is shown in Fig. 6. As can be seen from Fig. 6(a), adsorption capacity increases with increasing contact time and increases quickly during the first contact time of 4 h and then maintains a high level with increasing time. The rapid adsorption at the initial contact time can be attributed to the abundant availability of active sites on the HNTs-Fe_3O_4 surface [22]. Afterwards, with the gradual occupancy of these sites, the adsorption efficiency becomes less efficient. The quick adsorption of UO_2^{2+} on HNTs-Fe_3O_4 suggests that it is dominated by chemical adsorption/surface complexation rather than physical adsorption. In the following experiments, 12 h is chosen to achieve the adsorption equilibrium.

To analyze UO_2^{2+} kinetic adsorption on HNTs-Fe_3O_4, a pseudo-second-order rate equation is used to simulate the kinetic adsorption [31,32]:

$$\frac{t}{q_t} = \frac{1}{kq_e^2} + \frac{1}{q_e}t \quad (3)$$

where q_t (mg·g^{-1}) is the amount of UO_2^{2+} adsorbed on the surface of HNTs-Fe_3O_4 at time t (h), and q_e (mg·g^{-1}) is the equilibrium adsorption capacity. k (g·(mg·h)$^{-1}$) is the rate constant of pseudo-second-order kinetics. A linear plot of t/q_t versus t is shown in the inserted figure of Fig. 6(b).

The k and q_e values calculated from the slope and intercept of the linear plot of t/q_t versus t are 0.06 g·(mg·h)$^{-1}$ and 58.58 mg/g, respectively. The correlation coefficient (R^2) of the pseudo-second-order rate equation for the linear plot is very close to 1 (R^2=0.999), indicating that the kinetic adsorption of UO_2^{2+} on HNTs-Fe_3O_4 can be described by the pseudo-second-order rate equation well.

4. Effect of pH and Ionic Strength

Adsorption of UO_2^{2+} onto HNTs-Fe_3O_4 is studied by 0.001 M, 0.01 M and 0.1 M NaCl solutions, respectively. Experiments within the pH range of 2-11 are determined. The result is given in Fig. 7.

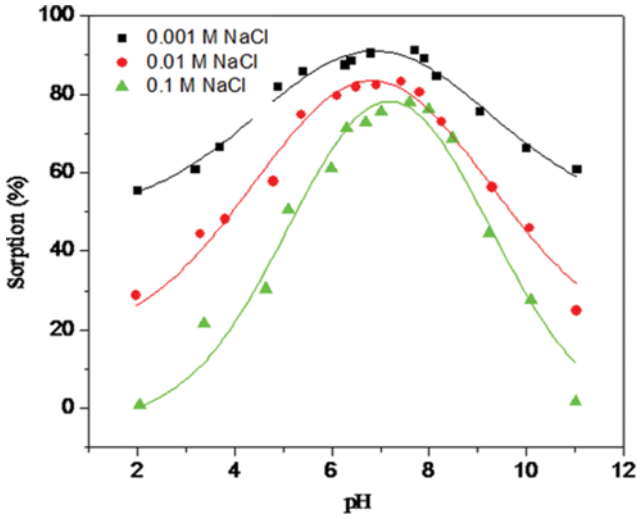

Fig. 7. Effect of ionic strength on UO_2^{2+} adsorption to HNTs-Fe_3O_4 at different pH values (T=293.15 K, m/V=0.968 g/L, C_0 (UO_2^{2+}) =6.452×10^{-6} mol/L).

It is evident that the adsorption of UO_2^{2+} is strongly affected by pH values. The adsorption of UO_2^{2+} on HNTs-Fe_3O_4 increases gradually with increasing pH at pH<7, reaches the highest adsorption at pH=7.5, and then decreases with increasing pH at pH>7.5. The highly pH and ionic strength dependent adsorption obvious that UO_2^{2+} adsorption is dominated by ion exchange, surface complexation and manifests various adsorption mechanisms [33,34].

The relative species of U(VI) as a function of pH values are shown in Fig. 8. At pH<4, UO_2^{2+} is the predominant species. At the pH range of 4-7.5, the main species are UO_2^{2+}, $UO_2(OH)_2^{2+}$, $UO_2(OH)^+$, $(UO_2)_3(OH)^{5+}$ and $(UO_2)_4(OH)^{7+}$, and the prominent species are $(UO_2)_3(OH)^{7-}$, $UO_2(OH)^{3-}$ and $UO_2(OH)_4^{2-}$ when pH>7.5.

The surface of HNTs-Fe_3O_4 becomes more negatively charged with the increasing of pH. The electrostatic attraction between positively charged UO_2^{2+}, $(UO_2)_3(OH)^{5+}$, $(UO_2)_4(OH)^{7+}$ and negatively charged surface of HNTs-Fe_3O_4 becomes strong, thus causing an increase of U(VI) adsorption on HNTs-Fe_3O_4 at pH<7 [35]. The decreasing of UO_2^{2+} adsorption on Fe_3O_4-HNTs at pH>7.5 might

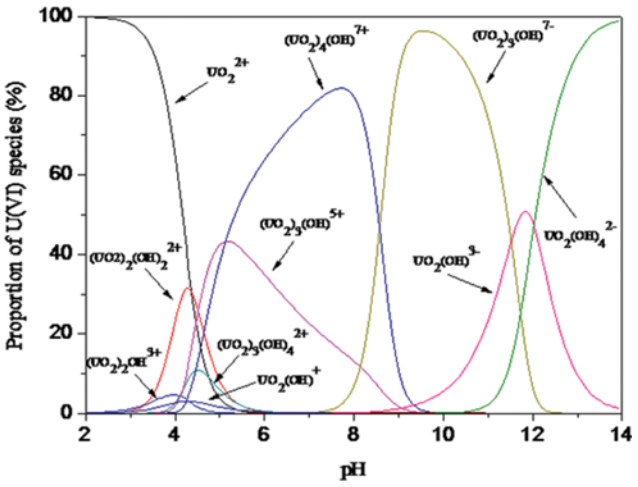

Fig. 8. Distribution of U(VI) species as a function of pH.

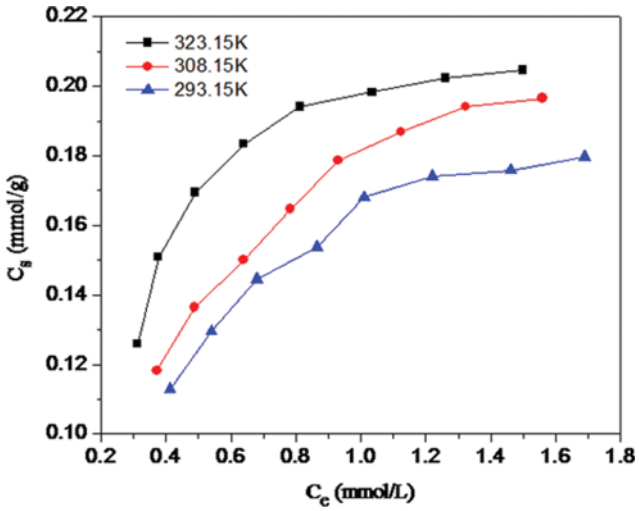

Fig. 9. Adsorption isotherms of UO_2^{2+} on Fe_3O_4-HNTs at three different temperatures (pH=5.5±0.1, m/V=0.484 g/L, I=0.01 M NaCl).

be explained by the electrostatic repulsion between $UO_2(OH)_4^{2-}$, $(UO_2)_3(OH)^{7-}$, $UO_2(OH)^{3-}$ and negative surface of HNTs-Fe_3O_4 at high pH values [36].

Fig. 7 also indicates the effect of ionic strength on UO_2^{2+} adsorption as a function of pH values. The adsorption of UO_2^{2+} is the highest in 0.001 M NaCl solution, and the lowest in 0.1 M NaCl solution. It is obvious that the ion exchange contributes to the adsorption of UO_2^{2+} from aqueous solution to HNTs-Fe_3O_4. The adsorption of UO_2^{2+} is mainly via ion exchange with hydrogen and sodium ions that saturate the exchange sites of HNTs-Fe_3O_4 [7,37]. The ion-exchange reactions can be expressed by the following reactions:

(1) Exchange with hydrogen ions:

$$\equiv SOH + UO_2^{2+} \rightarrow \equiv SOUO_2^{2+} + H^+ \quad (4)$$

$$2\equiv SOH + UO_2^{2+} \rightarrow (\equiv SO)_2UO_2^{2+} + 2H^+ \quad (5)$$

$$\equiv SOH_2^+ + UO_2^{2+} \rightarrow \equiv SOHUO_2^{2+} + H^+ \quad (6)$$

$$2\equiv SOH_2^+ + UO_2^{2+} \rightarrow (\equiv SOH)_2UO_2^{2+} + 2H^+ \quad (7)$$

(2) Exchange with Na^+ ions:

$$\equiv SONa + UO_2^{2+} \rightarrow \equiv SOUO_2^{2+} + Na^+ \quad (8)$$

$$2\equiv SONa + UO_2^{2+} \rightarrow (\equiv SO)_2UO_2^{2+} + 2Na^+ \quad (9)$$

(3) The hydrolysis of UO_2^{2+} in solution:

$$UO_2^{2+} + n\ H_2O \rightarrow [UO_2(H_2O)_{n-m}]^{2-m} + m\ H^+ \quad (10)$$

Since n>m, and exchange with hydrolyzed species:

$$\equiv SOH + UO_2(OH)_m(H_2O)_{n-m}^{2-m} \rightarrow \equiv SOUO_2(OH)_m^{1-m} + H^+ + (n-m)\ H_2O \quad (11)$$

5. Effect of Temperature and Thermodynamic Study

Fig. 9 shows the adsorption capacity of UO_2^{2+} onto HNTs-Fe_3O_4 at 293.15, 308.15, and 323.15 K, respectively. It is clear that the temperature has important effect on the adsorption process. The adsorption isotherm is the highest at 323.15 K and the lowest at 293.15 K. The adsorption capacity of UO_2^{2+} onto HNTs-Fe_3O_4 is found to increase with increase in temperature, indicating the process to be endothermic in nature. To prove the above views the equilibrium data is analyzed by the Langmuir, Freundlich, and Dubinin-Radushkevich (D-R) models in this study.

The Langmuir adsorption is based on the assumption of monolayer adsorption on a structurally homogeneous adsorbent. The linear form of Langmuir equation can be written as follows [38]:

$$\frac{C_e}{C_s} = \frac{1}{bC_{s\,max}} + \frac{C_e}{C_{s\,max}} \quad (12)$$

where C_e is the equilibrium concentration of UO_2^{2+} remaining in solution (mol/L); C_s is the amount of UO_2^{2+} adsorbed on per weight unit of HNTs-Fe_3O_4 after equilibrium (mol/g); $C_{s\,max}$ is the amount of UO_2^{2+} at complete monolayer coverage (mol/g), and is the maximum adsorption capacity; b (L/mol) is the Langmuir adsorption equilibrium constant.

The linear form of the Freundlich equation usually expressed as follows [39]:

$$\log C_s = \log K_F + n \log C_e \quad (13)$$

where K_F ($mol^{1-n}/L^n/g$) is the adsorption capacity when UO_2^{2+} equilibrium concentration equals to 1 and n represents the degree of dependence of adsorption with equilibrium concentration.

The D-R isotherm can be used to describe adsorption on both homogeneous and heterogeneous surfaces. The linear form of D-R equation has the general expression as [40]:

$$\ln C_s = \ln C_{s\,max} - \beta\varepsilon^2 \quad (14)$$

where C_s and $C_{s\,max}$ are defined above, β represents the activity coefficient related to the mean adsorption energy (mol^2/kJ), ε represents the Polanyi potential, which is equal to:

$$\varepsilon = RT \ln\left(1 + \frac{1}{C_e}\right) \quad (15)$$

where R is ideal gas constant (8.3145 J/mol·K^{-1}); T is the absolute temperature in Kelvin (K). E (kJ/mol) is the free energy change and it is required to transfer 1 mol of ions from solution to the solid surfaces. The equation is usually expressed as follows:

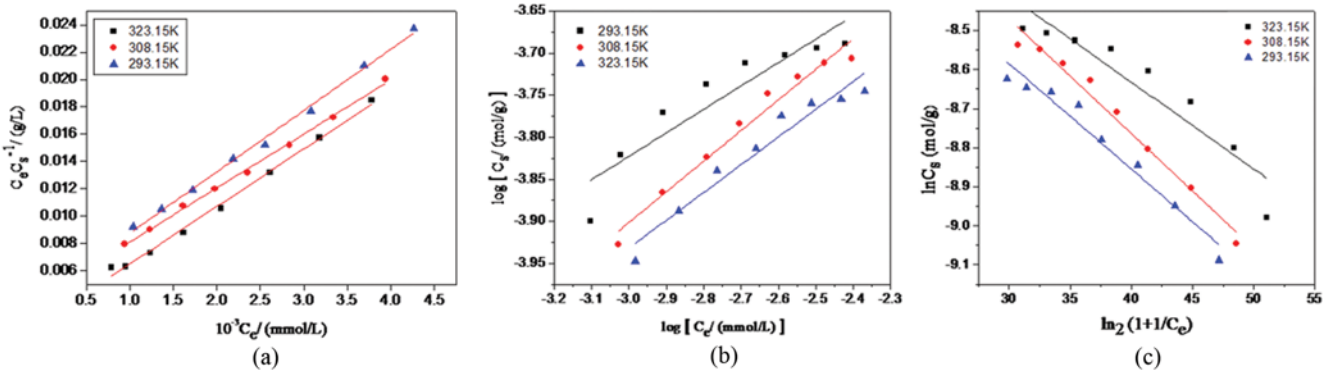

Fig. 10. Langmuir (a), Freundlich (b) and D-R (c) isotherms of UO_2^{2+} adsorption on HNTs-Fe_3O_4 at three different temperature (pH=5.5± 0.1, m/V=0.484 g/L, I=0.01 M NaCl).

Table 1. The parameters for Langmuir, Freundlich and D-R isotherms at different temperatures

T (K)	Langmuir			Freundlich			D-R		
	$C_{s\,max}$ (mmol/g)	b (L/mol)	R^2	K_F (mol^{1-n}/L^n/g)	n	R^2	β (mol^2/kJ)	$C_{s\,max}$ (mol/g)	R^2
293.15	0.223	1.05×10^3	0.996	1.03×10^{-3}	0.279	0.840	0.027	4.21×10^{-4}	0.957
308.15	0.253	9.48×10^2	0.997	1.56×10^{-3}	0.365	0.967	0.029	5.06×10^{-4}	0.975
323.15	0.238	1.81×10^3	0.994	1.14×10^{-3}	0.330	0.940	0.022	4.33×10^{-4}	0.865

$$E = \frac{1}{\sqrt{2\beta}} \quad (16)$$

The three models of isotherm plots for UO_2^{2+} adsorption onto HNTs-Fe_3O_4 are in Fig. 10. The relative values calculated from the three models are listed in Table 1. From R^2 values, one can conclude that the experimental data fits the Langmuir model better than Freundlich and D-R models. The Langmuir isotherm fits the experimental data well, demonstrating that it is monolayer adsorption on the structurally homogeneous HNTs-Fe_3O_4 [41]. Furthermore, the adsorption isotherm is the highest at 323.15 K and the lowest at 293.15 K. The result indicates that high temperature is beneficial to the adsorption process. The value of n acquired from the Freundlich model is lower than 1, which indicates that nonlinear adsorption takes place on HNTs-Fe_3O_4 surface. The E values obtained from Eq. (8) are 4.303 (T=293.15 K), 4.124 (T=308.15 K), 4.746 (T=323.15 K) kJ/mol, which are in the adsorption energy range of chemical ion-exchange reaction [42]. The parameters calculated from the analysis of the three isotherm models demonstrate that the adsorption of UO_2^{2+} onto Fe_3O_4-HNTs is a beneficial and chemisorption process. In addition, we also compared the UO_2^{2+} adsorption capacity of the Halloysite nanotube-Fe_3O_4 composite with other adsorbents as shown in Table 2.

Table 2. UO_2^{2+} adsorption capacity of halloysite nanotube-Fe_3O_4 compared with other adsorbents

Adsorbent	Adsorption capacity (mg/g)	References
Bentonite	36.4	[19]
FeO nanoparticle	85.35	[43]
FeO-NH nanoparticle	268.49	[43]
Triphosphate-cross linked magnetic chitosan resins	169.5	[44]
Bayberry tannin	56.8	[45]
Black wattle tannin immobilized membranes	53.0	[45]
Halloysite nanotube-Fe_3O_4	88.32	This study

The thermodynamic constants ΔH^0, ΔG^0, ΔS^0 for UO_2^{2+} adsorption on Fe_3O_4-HNTs can be obtained from the temperature-dependent adsorption isotherms. The values of enthalpy change ΔH^0 and entropy change ΔS^0 are calculated from the slope and intercept of the plot of lnK_d versus 1/T (Fig. 11) via applying the following equation [46]:

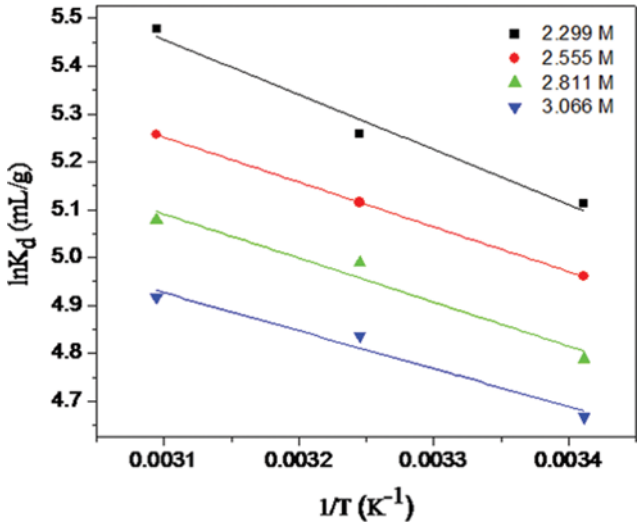

Fig. 11. Linear plots of lnK_d vs. C_e of UO_2^{2+} adsorption onto HNTs-Fe_3O_4 (pH=5.5±0.1, m/V=0.484 g/L, I=0.01 M NaCl).

Table 3. The thermodynamic data of UO_2^{2+} adsorption on Fe_3O_4-HNTs at different initial concentrations

C_0 (mol/L)	ΔS^0 (J/(mol·K))	ΔH^0 (kJ/mol)	ΔG^0 (kJ/mol)		
			293.15 K	308.15 K	323.15 K
2.299	74.898	9.532	−12.424	−13.548	−14.671
2.555	67.728	7.765	−12.089	−13.105	−14.121
2.811	66.028	7.646	−11.710	−12.701	−13.691
3.066	61.396	6.593	−11.405	−12.326	−13.247

$$\ln K_d = \frac{\Delta S^0}{R} - \frac{\Delta H^0}{RT} \quad (17)$$

The change of Gibbs free energy (ΔG^0) is calculated from the equation:

$$\Delta G^0 = \Delta H^0 - T\Delta S^0 \quad (18)$$

The thermodynamic data acquired from Eqs. (9) and (10) are listed in Table 3. The positive enthalpy change (ΔH^0) shows that the adsorption process of UO_2^{2+} is endothermic. The adsorption of UO_2^{2+} may require at least a partial decomposition of their hydration shell, and this process needs energy [47]. This energy exceeds the exothermicity of cations to attach to the solid surface [48,49]. The adsorption of UO_2^{2+} requires a diffusion process, which is endothermic. The negative values of ΔG^0 indicate that the UO_2^{2+} adsorption on HNTs-Fe_3O_4 is spontaneous, and the value of ΔG^0 decreased with increasing temperature. This phenomenon indicates that a higher temperature is favorable for adsorption. The positive values of entropy change (ΔS^0) means randomness is increased at the solid/solution interface during the adsorption.

CONCLUSIONS

Based on the experimental results of UO_2^{2+} adsorption on HNTs-Fe_3O_4, we reached the following conclusions: (1) The experimental results demonstrate that the adsorbents with HNTs-Fe_3O_4, at T= 298.15 K, m/V=0.484 g/L and with a solution pH=5.5±0.1, have the largest adsorption capacity of 88.32 mg/g for UO_2^{2+}, indicating the adsorbent is effective for UO_2^{2+} removal. (2) The adsorption of UO_2^{2+} on Fe_3O_4-HNTs is rather fast and the isotherm adsorption data is well fitted by the Langmuir model. Furthermore, the kinetic data is well fitted by the pseudo-second-order model. (3) The adsorption of UO_2^{2+} onto HNTs-Fe_3O_4 is strongly dependent on pH. The adsorption of UO_2^{2+} increased quickly with increasing pH at pH<7.5, and decreased with increasing pH at pH>7.5. (4) The negative values of ΔG^0 and ΔH^0 show that the adsorption is spontaneous and endothermic.

ACKNOWLEDGEMENTS

The work was supported by the National Natural Science Foundation of China (20967006), and Education Ministry's New Century Excellent Talents Supporting Plan (NCET-07-0476).

REFERENCES

1. D. D. Shao, Z. Jiang, X. Wang, J. Li and Y. Meng, *J. Phys. Chem B.*, **113**, 860 (2009).
2. S. Sachs and G. Bernhard, *Chemosphere*, **72**, 1441 (2008).
3. M. H. Baik, W. J. Cho and P. S. Hahn, *J. Radioanal. Nucl. Chem.*, **260**, 495 (2004).
4. X. M. Ren, C. L. Chen, N. Masaaki and X. K. Wang, *Chem. Eng. J.*, **170**, 395 (2011).
5. Y. L. Chi, Y. T. Chen, X. Liu, Z. J. Guo and L. S. Cai, *J. Radioanal. Nucl. Chem.*, **292**, 1349 (2012).
6. D. D. Shao, J. Hu and X. K. Wang, *Plasma. Process. Polym.*, **7**, 977 (2010).
7. J. Hu, D. D. Shao, C. L. Chen, G. D. Sheng, J. X. Li, X. K. Wang and M. Nagatsu, *J. Phys. Chem B.*, **114**, 6779 (2010).
8. S. B. Yang, J. Hu, C. L. Chen, D. D. Shao and X. K. Wang, *Environ. Sci. Technol.*, **45**, 3621 (2011).
9. H. Zhang, L. Chen, L. P. Zhang and X. J. Yu, *J. Radioanal. Nucl. Chem.*, **287**, 357 (2010).
10. Q. H. Fan, X. L.Tan, J. X. Li, X. K. Wang, W. S. Wu and G. Montavon, *Environ. Sci. Technol.*, **43**, 5776 (2009).
11. Q. H. Fan, D. D. Shao, W. S. Wu and X. K. Wang, *Chem. Eng. J.*, **150**, 188 (2009).
12. Z. J. Liu, L. Chen, Y. H. Dong and Z. C. Zhang, *J. Radioanal. Nucl. Chem.*, **289**, 851 (2011).
13. G. D. Sheng, S. W. Wang, J. Hu, Y. Lu, J. X. Li, Y. H. Dong and X. K. Wang, *Colloids Surf., A.*, **339**, 159 (2009).
14. G. X. Zhao, L. Jiang, Y. D. He, J. X. Li, H. L. Dong, X. K. Wang and W. P. Hu, *Adv. Mater.*, **23**, 3959 (2011).
15. G. X. Zhao, X. M. Ren, X. Gao, X. L. Tan, J. X. Li, C. L. Chen, Y. Y. Huang and X. K. Wang, *Dalton. Trans.*, **40**, 10945 (2011).
16. P. Luo, Y. F. Zhao, B. Zhang, J. D. Liu, Y. Yang and J. F. Liu, *Water Res.*, **44**, 1490 (2010).
17. Y. Du and P. Zheng, *Korean J. Chem. Eng.*, **31**, 2051 (2014).
18. P. Luo, B. Zhang, Y. Zhao, J. Wang, H. Zhang and J. Liu, *Korean J. Chem. Eng.*, **28**, 800 (2011).
19. J. Xiao, Y. T. Chen, W. H. Zhao and J. B. Xu, *J. Mol. Liq.*, **188**, 184 (2013).
20. V. Rocher, J. M. Siaugue, V. Cabuil and A. Bee, *Water Res.*, **42**, 1291 (2008).
21. V. K. Gupta, S. Agarwal and T. A. Saleh, *Water Res.*, **45**, 2208 (2011).
22. J. M. Duan, R. C. Liu, T. Chen, B. Zhang and J. Liu, *Desalination*, **293**, 46 (2012).
23. Y. F. Xie, D. Y. Qian, D. L. Wu and X. F. Ma, *Chem. Eng.*, **168**, 960 (2011).
24. P. Luo, Y. F. Zhao, B. Zhang, J. D. Liu, Y. Yang and J. F. Liu, *Water Res.*, **44**, 1490 (2010).
25. E. Tierrablanca, J. Romero-Garcia, P. Roman and R. Cruz-Silva, *Appl. Catal. A: Gen.*, **381**, 270 (2010).
26. S. T. Yang, P. F. Zong, J. Hu, G. D. Sheng and X. K. Wang, *Chem. Eng. J.*, **214**, 378 (2013).
27. Z. G. Liu, F. S. Zhang and R. Sasai, *Chem. Eng. J.*, **160**, 59 (2010).
28. Y. F. Xie, D. Y. Qian, D. L. Wu and X. F. Ma, *Chem. Eng. J.*, **168**, 961 (2011).
29. D. Lee, R. E. Cochen and M. F. Rubner, *Langmuir*, **23**, 127 (2007).
30. P. Chang, S. Yu, T. Chen, A. Ren, C. Chen and X. Wang, *J. Radioanal. Nucl. Chem.*, **274**, 155 (2007).
31. C. L. Chen and X. K. Wang, *Ind. Eng. Chem. Res.*, **45**, 9144 (2006).
32. X. L. Wu, L. Wang, C. L. Chen, A. W. Xu and X. K. Wang, *J. Mas-*

ter. Chem., **21**, 17353 (2011).
33. S. S. Lu, Z. Q. Guo, C. C. Zhang and S. W. Zhang, *J. Radioanal. Nucl. Chem*., **287**, 621 (2011).
34. X. L. Tan, J. Hu, M. Gilles and X. K. Wang, *Dalton. Trans*., **40**, 10953 (2011).
35. M. F. Zhao and P. Liu, *Micropor. Mesopor. Mater.*, **112**, 421 (2008).
36. T. Arnold, T. Zorm, H. Zänker, G. Bernhard and H. Nitsche, *J. Contam. Hydrol*., **47**, 219 (2001).
37. C. L. Chen, J. Hu, D. D. Shao, J. X. Li and X. K. Wang, *J. Hazard. Mater*., **164**, 923 (2009).
38. R. C. Liu, B. Zhang, D. D. Mei, H. Q. Zhang and J. D. Liu, *Desalination*, **268**, 112 (2011).
39. A. B. Zhang, L. Pan, H. Y. Zhang, S. T. Liu, Y. Ye, M. S. Xia and X. G. Chen, *Colloids and Surfaces A: Physicochem. Eng. Aspects*., **396**, 186 (2012).
40. F. N. Behdani, A. T. Rafsanjani, M. Torab-Mostaedi and S. M. A. K. Mohammadpour, *Korean J. Chem. Eng*., **30**, 448 (2013).
41. X. L. Tan, X. K. Wang, M. Fang and C. L. Chen, *Colloids Surf., A*., **296**, 113 (2007).
42. A. öZcan, E. M. Öncü and A. S. öZcan, *Colloids Surf., A*., **277**, 94 (2006).
43. G. Peng, D. Ding, F. Xiao, X. Wang, N. Hun, Y. Wang, Y. Dai and Z. Cao, *J. Radioanal. Nucl. Chem*., **301**, 781 (2014).
44. L. M. Zhou, Y. Y. Jia, J. Peng, Z. R. Liu and E. Al-Zaini, *J. Radioanal. Nucl. Chem*., **302**, 331 (2014).
45. X. P. Liao, H. W. Ma, R. Wang and B. Shi, *J. Membr. Sci*., **243**, 235 (2004).
46. H. I. Adegoke, F. AmooAdekola, O. S. Fatoki and B. J. Ximba, *Korean J. Chem. Eng*., **31**, 142 (2014).
47. S. S. Tahir and N. Rauf, *Chem. Thermodyn*., **35**, 2006 (2003).
48. L. M. Zuo, S. M. Yu, H. Zhou, J. Jiang and X. Tian, *J. Radioanal. Nucl. Chem*., **288**, 581 (2011).
49. X. L. Wu, L. Wang, C. L. Chen, A. W. Xu and X. K. Wang, *J. Mater. Chem*., **21**, 17357 (2011).